

DESIGN OF AN EMPIRICAL PROCESS MODEL AND ALGORITHM FOR THE TUNGSTEN INERT GAS WIRE+ARC ADDITIVE MANUFACTURE OF Ti-6Al-4V COMPONENTS

Filomeno Martina^{*,a}, Stewart W. Williams^{*}, Paul Colegrove^{*}

^{*}Welding Engineering and Laser Processing Centre (WELPC), Cranfield University, Cranfield,
MK43 0AL, United Kingdom

^af.martina@cranfield.ac.uk

Abstract

In the wire+arc additive manufacture process parameters can be varied to achieve a wide range of deposit widths, as well as layer heights. Pulsed Tungsten Inert Gas was chosen as the deposition process. A working envelope was developed, which ensures unfeasible parameters combinations are excluded from the algorithm. Thanks to an extensive use of a statistically designed experiment, it was possible to produce process equations through linear regression, for both wall width and layer height. These equations are extremely useful for automating the process and reducing the buy-to-fly ratio. For a given layer height process parameters can be selected to achieve the required layer width while maximising productivity.

1 Introduction

Additive manufacturing (AM) is one of the emerging innovative manufacturing approaches. Formerly a rapid prototyping technique, it is been considered as a manufacturing technique in its own right, particularly within aerospace and more recently automotive sectors. Wire+arc additive manufacturing (WAAM) [1] is one of the many AM processes, and it consists in the utilisation of arc welding tools for AM purposes. Different from laser-based processes, which use only one set of deposition parameters and have fixed values for layer height, hatch distance, etc, WAAM offers the possibility of changing the deposition parameters on an *ad hoc* basis. Almeida and Williams [1] were the first to relate the process parameters to the geometry of the material deposited, for Ti-6Al-4V, while using an innovative metal inert gas (MIG) approach, namely Cold Metal Transfer (CMT). The model enabled the flexible selection of deposition parameters that changed according to the desired geometry; for instance, to achieve a certain wall width or layer height, a specific combination of process parameters would be selected. It must be noted that to minimise material waste, being able to deposit a geometry that is as close as possible to the final one is highly beneficial.

The scope of the present work is to determine a model that relates process parameters to weld bead geometry, for tungsten inert gas (TIG) based WAAM. Moreover, this work addresses a feasibility issue by determining a working envelope for the process, which excludes the unfeasible parameters combinations.

2 Experimental method

An EWM Plasma/TIG power source and an EWM TIG torch mounted on an ABB 6-axes robot were used for the deposition. A 100 mm long trailing shield was used to minimise oxidation by applying argon gas locally. The 1.2 mm wire was always front-fed; a schematic of the setup is shown in Fig. 1. After a preliminary assessment of the significance of all the parameters, some of them were kept constant to reduce the number of independent variables investigated, and therefore the complexity of the experiment (see Table. 1). Gas flow rates were also kept constant (Table 2).

To determine the process window, a visual, qualitative analysis of 70 preliminary single layer (bead on plate) experiments provided the necessary information for understanding the general behaviour of the process and determining the limitations of the process parameters, as well as excluding the unfeasible parameters combinations.

After establishing the process constraints, a D-Optimal design method [2] was chosen for the experiment, given its capability of taking constraints into account and supporting irregular experimental regions. Wire feed speed (WFS) [X_1], travel speed (TS) [X_2] and current (I) [X_3] were selected as the factors in the model. WFS is the speed (m min^{-1}) at which wire is fed into the molten pool (Fig. 1); TS is the travel speed (mm s^{-1}) of the manipulator (and consequently of the torch) along the X axis; and I (A) influences the heat input. 21 straight parts were made of 15 layers each and were 250 mm long. Layer deposition always started from the same end. The part was allowed to cool down to 50°C before depositing a new layer for consistent part geometry.

Three-factor second-order polynomial functions were fitted to each of the responses:

$$Y = \beta_0 + \sum_{i=1}^3 \beta_i x_i + \sum_{i < j}^3 \beta_{ij} x_i x_j + \sum_{i=1}^3 \beta_{ii} x_i^2 \quad (1)$$

where Y is the predicted response, β_0 is the constant process effect, β_i is the linear effect of x_i , β_{ij} are the interactions of first order and β_{ii} are the quadratic effects of x_i .

2.1 Measurements

Three transverse sections were used for the measurements. During the build process, the deposited layer height (LH) was measured at 50 mm, 100 mm and 150 mm from the deposition starting point. The average was used to determine the height increment for deposition of the following layer. For the statistical analysis, given the thermal effect of the base plate, the first four layers were analysed one by one (LH₁, LH₂, LH₃ and LH₄, as shown in Fig. 2) and for the remaining layers, i.e. from the 5th to the 15th, their overall average was considered:

$$LH = \frac{LH_5 + LH_6 + \dots + LH_{15}}{11} \quad (2)$$

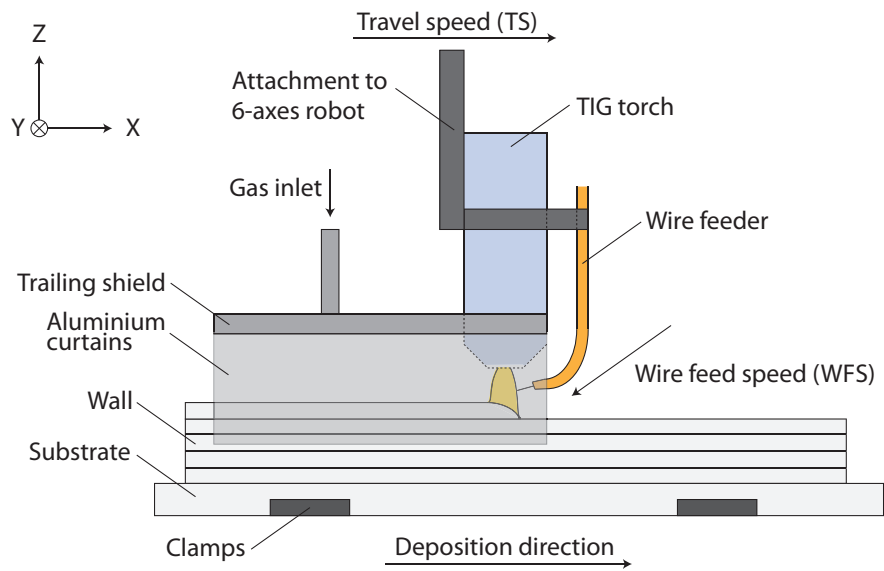


Figure 1: Schematic of experimental setup.

Table 1: Values for the process parameters which were excluded during the factors selection and therefore kept constant.

Electrode-to-workpiece distance	3.5 mm
Tungsten electrode tip angle	30°
Wire diameter	1.2 mm
I_p/I_b^*	1.5
Pulses duration	0.05 s
Frequency	10 Hz

* I_p and I_b are peak and background currents

Table 2: Deposition stages: gas flow rate, and durations.

	Pre purge	Slope up	Deposition	Slope down	Post purge
Process gas flow rate ($l \text{ min}^{-1}$)	9	9	9	9	9
Trailing shield gas flow rate ($l \text{ min}^{-1}$)	20	20	20	20	20
Duration (s)	10	0.1	42 to 125 ^a	0.1	20

^aDuration depended on the travel speed

Also the wall widths (WW) were considered separately, according to their dependence on the layer height. To do this, a series of parallel lines was laid, orientated in the Y direction parallel to the baseplate, on the optical microscope images of the three sections, each line corresponding to a specific layer height. Consequently, it became possible to infer the shape of the wall for every layer, and a WW could be associated with each of them. As well as in the LH measurements, the first four WW were measured separately (WW_1 , WW_2 , WW_3 and WW_4) considering the narrowest point, while the remaining part of the wall was considered as a whole. Furthermore, for the overall WW (equation 3) the average of the measurements of the three transverse sections was considered:

$$WW = \frac{WW_a + WW_b + WW_c}{3} \quad (3)$$

where WW_a is the width of the section taken at 50 mm, WW_b of the 100 mm one, and WW_c of the 150 mm one. The wall widths of the first four layers (WW_1 to WW_4) used only the central transverse section.

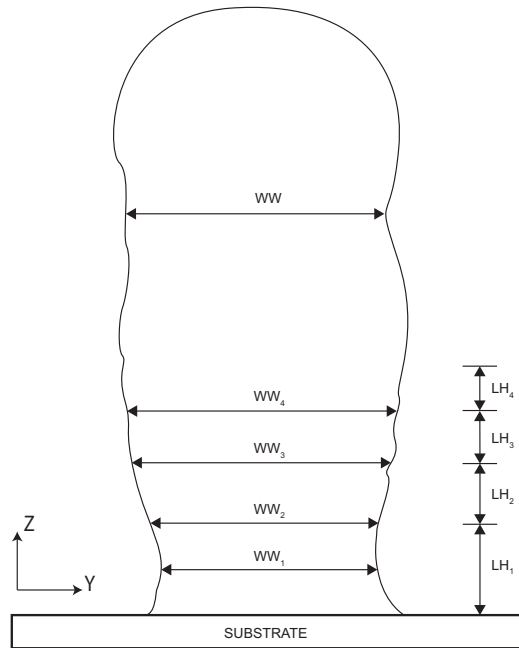


Figure 2: Schematic representation of a generic part cross-section. The wall width (WW) takes into account the width of the specimen, at its minimum point, for the first four layers separately and then for the remaining part as a whole. The layer height (LH) corresponds to the increase in specimen's height after the deposition of a new layer. The first four layers were considered separately.

3 Experimental results and discussion

3.1 Working envelope

The constraints on the parameters are represented by the solid lines in Fig. 3. To ensure additional confidence on process reliability and feasibility, the strength of the constraints b, e, d, f was increased by 10% (dashed lines in Fig. 3). Note the current considered in the design of experiment is the average one, given by the average of I_p and I_b described in Section 2.

3.2 Process capability

The ranges of measured responses are shown in Fig. 4a, and a comparison against competing processes is shown in Fig. 4b. The comparison data, which for the CMT and plasma wire deposition (PWD) processes considers only out-of-chamber manufacturing methods, is taken from the work of Almeida and Williams [1], Martina et al. [4], Eze [5], Milewski et al. [6], Tolochko et al. [7]. Note that it was assumed that the wall width equalled the spot size for laser-based processes. Fig. 4a shows how the range of both WW and LH is quite consistent and does not vary depending on the layer number. In Fig. 4b, TIG deposition performs similarly to PWD, in terms of both WW and LH, although both are slightly smaller with TIG. The capability of TIG deposition is complementary to CMT, with the latter producing thinner walls with a much greater layer height. This suggests the possibility of combining the two processes to increase the overall capability of a manufacturing station. The main advantage of the powder-bed laser deposition process is the small feature size capability, however they are characterised by a much lower deposition rate, which ranges from 100 g h^{-1} to 200 g h^{-1} [4, 8].

Fig. 4c shows the ranges of wall widths that are achievable for each layer height. The minimum WW (around 5 mm) can be obtained for any LH between 0.6 mm to 1.4 mm. While the low WW

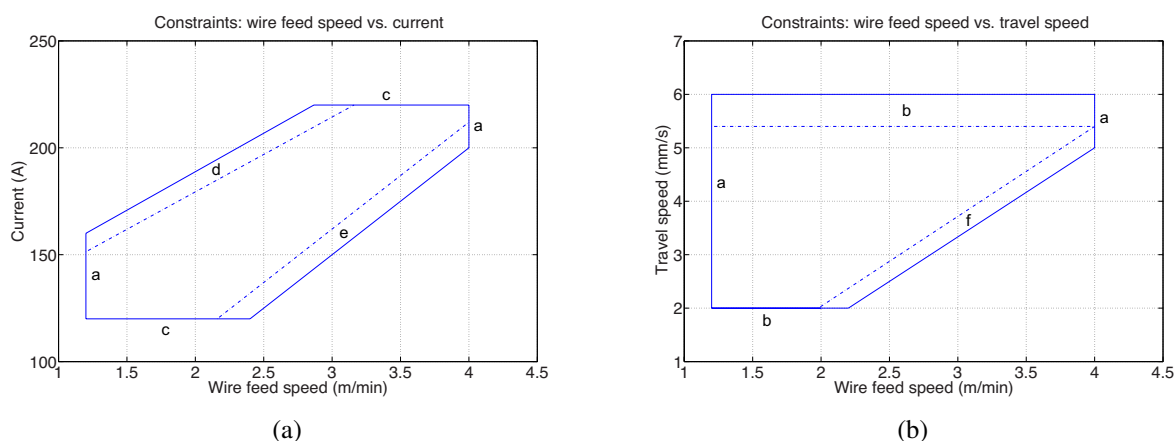
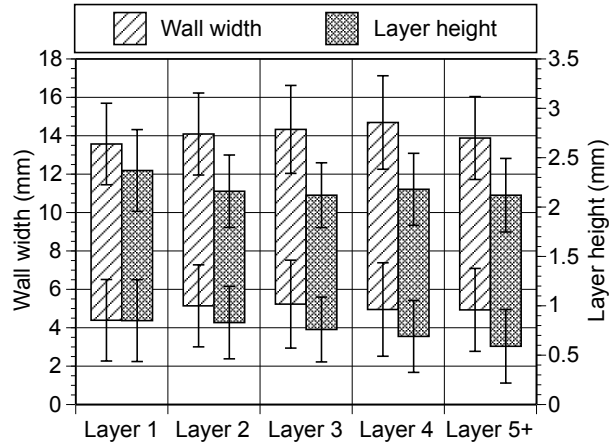
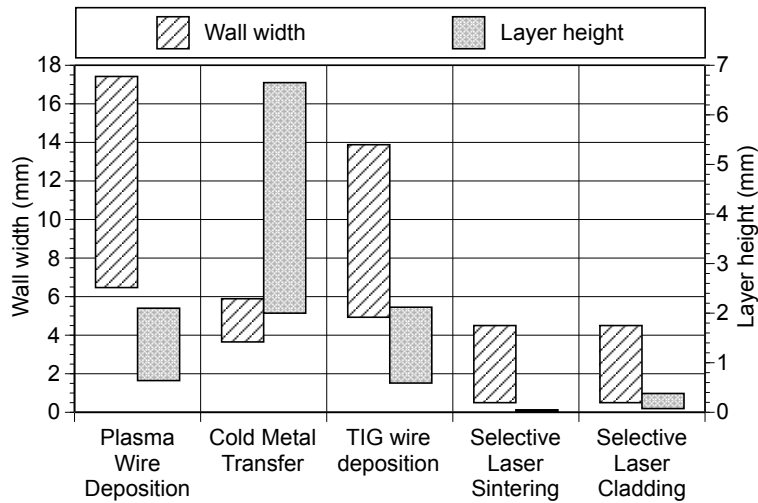


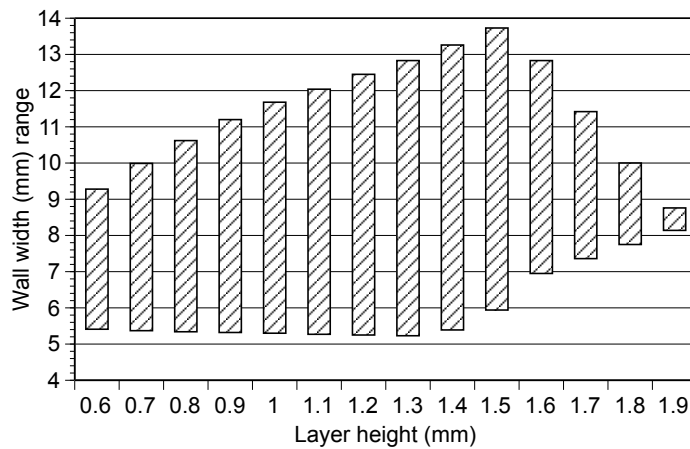
Figure 3: Working envelope for (a) wire feed speed - current and (b) wire feed speed - travel speed plans. The letters indicate the constraint each line refers to.



(a)



(b)



(c)

Figure 4: Process capability. (a) ranges of responses (error bars indicate standard deviations calculated by Stat-Ease Design-Expert 7.1® [3]); (b) comparison between TIG deposition and other AM processes (WW and LH responses are considered); and (c) wall width range vs. layer height.

value stays constant, the high value increases steadily and reaches its maximum at around 14 mm for a LH of 1.5 mm. For $LH > 1.5$ mm the WW range reduces progressively, and eventually for a LH of 1.9 mm the WW ranges from 8 mm to 9 mm only. The process flexibility enables layer height to be fixed for the whole part, while the WW may be varied according to the specific features that need building.

The maximum deposition rate achieved using TIG deposition was 1.2 kg h^{-1} ; however, it was constrained by the 4 m min^{-1} limit of the wire feeder used when doing the preliminary experiments (see Section 2). The time to deposit the 15 layers, considering deposition time only, ranged from 10 min 30 s to 31 min 15 s, and depended on travel speed (cooling time is ignored).

3.3 Statistical analysis and process equations calculation

To determine the relationship between the measured response and the statistically significant variables, analysis of variance (ANOVA) was performed. The responses are:

- wall widths of the first, second, third and fourth layers (respectively WW_1 , WW_2 , WW_3 and WW_4 all in [mm]);
- wall width of the remaining layers (WW in [mm]);
- height of the first, second, third and fourth layers (respectively LH_1 , LH_2 , LH_3 and LH_4 all in [mm]);
- height of the remaining layers (LH in [mm]).

3.3.1 Statistical tests

Table 3 presents the coefficients of determination (R^2) and adjusted- R^2 for the models. The R^2 coefficients, which according to Montgomery [2] measure the proportion of the variability in the data that can be explained by the model, indicate that over 90% of the variability can be explained by the models. In six cases it is over 95% and in five over 97%. In practice this should translate to good agreement between expected and actual dimensions. Pred- R^2 measures the variability explained by the model for new data and is in reasonable agreement with Adjusted- R^2 . Finally, the Adeq. Precision tests, which measure the signal-to-noise ratio, are greater than 4, which is the minimum value typically accepted for this term.

3.3.2 Analysis of plots

3D surfaces and contour plots were generated to represent graphically the regression equations. The WW (Fig. 5) does not seem to depend on the wire feed speed, and it is mostly affected by the

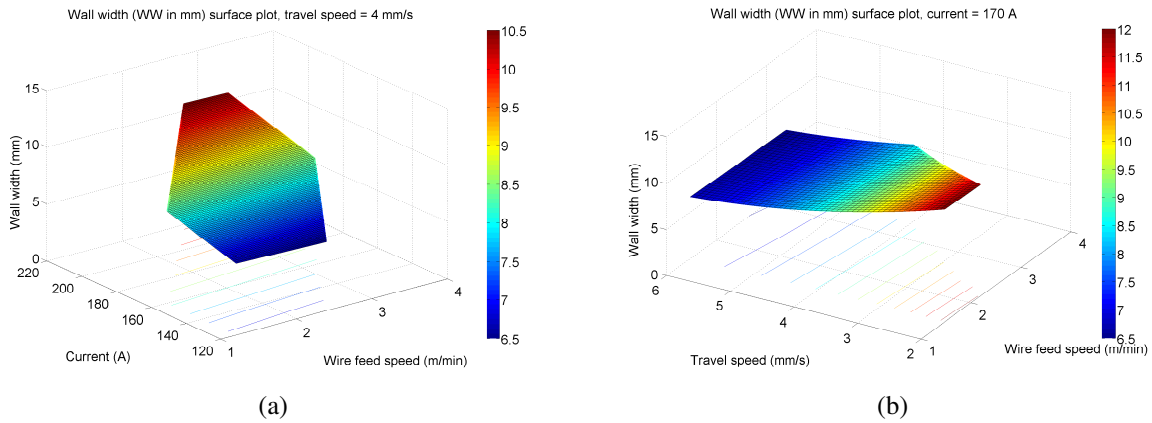


Figure 5: Wall width 3D surfaces. (a) wall width as a function of wire feed speed and current (travel speed = 4 mm s^{-1}), and (b) wall width as a function of wire feed speed and travel speed (current = 170 A).

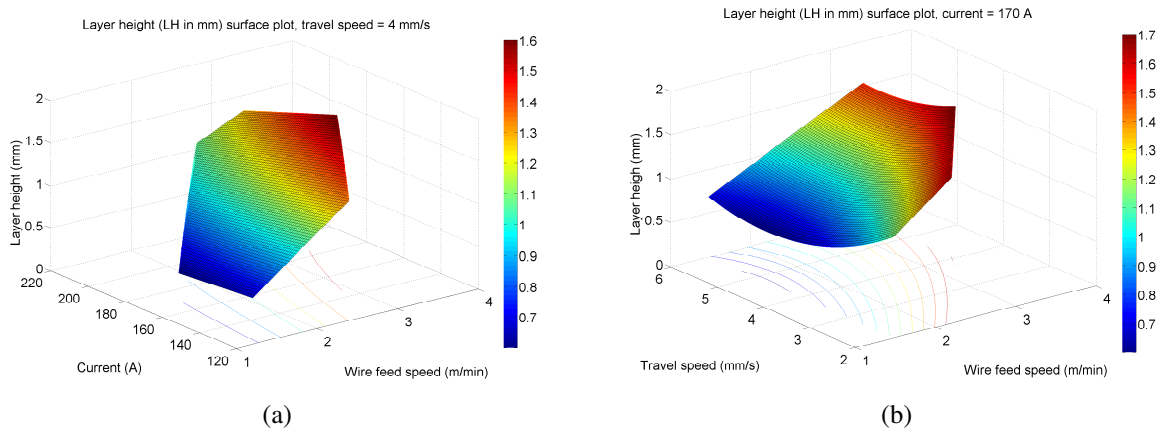


Figure 6: Layer height 3D surfaces. (a) layer height as a function of wire feed speed and current (travel speed = 4 mm s^{-1}), and (b) layer height as a function of wire feed speed and travel speed (current = 170 A).

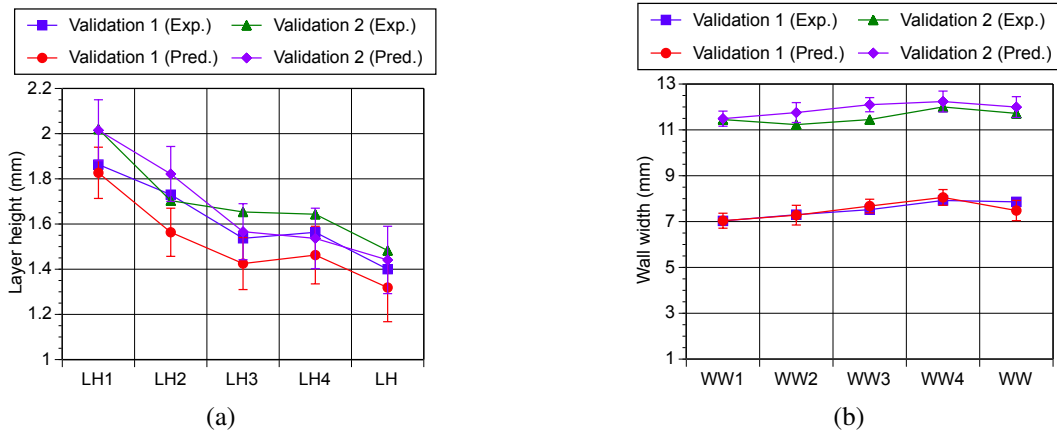


Figure 7: Comparison of experimental vs. predicted results for two specimens built in order to validate the calculated models. (a) evaluation of layer height models; (b) evaluation of wall width models. Error bars represent 95% confidence intervals.

Table 3: Statistical tests performed on the final models.

	R²	Adjusted – R²	Pred. – R²	Adeq. Precision	P-values
WW₁	0.987	0.9805	0.9576	47.849	<0.0001
WW₂	0.9776	0.9663	0.9228	34.901	<0.0001
WW₃	0.9922	0.9867	0.9679	47.329	<0.0001
WW₄	0.981	0.9724	0.9466	35.301	<0.0001
WW	0.9713	0.9611	0.9435	36.139	<0.0001
LH₁	0.9534	0.9224	0.8111	16.667	<0.0001
LH₂	0.9206	0.8941	0.83	20.408	<0.0001
LH₃	0.919	0.8816	0.7654	18.736	<0.0001
LH₄	0.9237	0.8884	0.7474	19.066	<0.0001
LH	0.901	0.8554	0.738	16.664	<0.0001

current and the travel speed. The lack of dependence on the wire feed speed is shown also by its p-value, which is 0.3870. The insensitivity to WFS in terms of WW is the main difference with plasma wire deposition. In fact, Martina et al. [4] showed how in plasma wire deposition an increase in wire feed speed results in an increase in wall width. On the contrary, the effect of travel speed and current is in agreement with what seen previously in plasma wire deposition [4]. Fig. 5b show the effect of the interaction of wire feed speed and travel speed. Also in this case the colouring suggests very little effect of wire feed speed, and the predominance of travel speed.

The LH results are plotted in Fig. 6. Unlike the WW, the wire feed speed affects the response. In the plot of the interaction of the wire feed speed with the travel speed (Fig 6b), the surface shows a more quadratic behaviour given by the effect of the travel speed.

The other modelled responses (WW₁, WW₂, WW₃, WW₄, LH₁, LH₂, LH₃ and LH₄) behave similarly to WW and LH, and therefore their specific plots aren't be included in this paper.

3.3.3 Model validation

To validate the models, two additional walls were built. For *Validation 1* the parameters were selected randomly within the working envelope, with WFS = 2.5 m min⁻¹, TS = 4 mm s⁻¹ and I = 150 A. For *Validation 2* the parameters were chosen so that a WW of 12 mm could be obtained, with WFS = 2.38 m min⁻¹, TS = 2.57 mm s⁻¹, I = 190 A. The measured values were compared with those predicted by Stat-Ease Design-Expert 7.1® [3], as shown in Fig. 7. All values fell within the calculated 95% confidence intervals, except for the LH₂ of the first specimen (underestimated), and WW₂–WW₃ of the second (overestimated).

4 Conclusions

In this research:

- A working envelope in which the process behaves steadily and delivers acceptable parts has been defined;
- TIG-based WAAM has been modelled empirically, through a systematic approach (design of experiment), and specifically D-Optimal design;
- Modelled responses include: LH, WW for the first four layers, and the average for the remaining ones;
- The model has been validated successfully.

In terms of process capability:

- Layer height ranged from 0.59 mm to 2.12 mm;
- Wall width ranged from 4.93 mm to 13.88 mm;
- Maximum deposition rate was 1.2 kg (limited by wire feeder).

From a statistical point of view:

- Wall width is highly dependant on the current;
- Layer height is dependant on wire feed speed.

Acknowledgements

The authors would like to thank Mr Flemming Nielsen and Mr Brian Brooks for their support during the research activities. Financial support from the EPSRC and EADS Innovation Works is also acknowledged.

References

- [1] P.M. Sequeira Almeida and S. Williams. Innovative process model of Ti-6Al-4V additive layer manufacturing using Cold Metal Transfer (CMT). In *21st International Solid Freeform Fabrication Symposium*, pages 25–36, Austin, Texas, USA, August 9-11 2010.
- [2] D.C. Montgomery. *Design and Analysis of Experiments*. John Wiley & Sons, fifth edition, 2006.
- [3] Stat-Ease Design-Expert 7.1®. <http://www.statease.com/dx71descr.html>, 2008.

- [4] F. Martina, J. Mehnen, S. W. Williams, P. Colegrove, and F. Wang. Investigation of the benefits of plasma deposition for the additive layer manufacture of Ti–6Al–4V. *Journal of Materials Processing Technology*, 212(6):1377–1386, June 2012.
- [5] E. Eze. VBC welding system parameter effect on the shape and microstructure of additively manufactured ti6al4v titanium alloy. Master’s thesis, Cranfield University, 2009.
- [6] J.O. Milewski, P.G. Dickerson, R.B. Nemeč, G.K. Lewis, and J.C. Fonseca. Application of a manufacturing model for the optimization of additive processing of Inconel alloy 690. *Journal Of Materials Processing Technology*, 91(1-3):18–28, 1999.
- [7] N.K. Tolochko, S.E. Mozzharov, I.A. Yadroitsev, T. Laoui, L. Froyen, V.I. Titov, and M.B. Ignatiev. Selective laser sintering and cladding of single-component metal powders. *Rapid Prototyping Journal*, 10(2):88–97, 2004.
- [8] H. Zhang, J.P. Xu, and G.L. Wang. Fundamental study on plasma deposition manufacturing. *Surface and Coatings Technology*, 171(1-3):112–118, 2003.